Dalton Transactions

Accepted Manuscript

ROYAL SOCIETY OF CHEMISTRY

www.rsc.org/dalton

Dalton Transactions

ARTICLE

Rare Earth Anthracenedicarboxylate Metal-Organic Frameworks: Slow Relaxation of Magnetization of Nd^{3+}, Gd^{3+}, Dy^{3+}, Er^{3+} and Yb^{3+} based Materials.

Received 00th January 20xx,
Accepted 00th January 20xx

DOI: 10.1039/x0xx00000x

www.rsc.org/

Antonio J. Calahorro,[a] Itziar Oyarzabal,[b] Belén Fernández,[a] José M. Seco,[b,*] Tian Tian,[c] David Fairen-Jimenez,[c] Enrique Colacio[a,*] and Antonio Rodríguez-Diéguez[a,*]

We have synthesized a novel family of metal-organic-frameworks (MOFs) based on the 9,10-anthracenedicarboxylate linker. We report the formation of lanthanides-based MOFs using soft solvothermal routes with dimethylformamide as solvent. These materials display intense photoluminescence properties in the solid state at room temperature. What is more interesting, some of them exhibit slow relaxation of magnetization with activation barriers of 22.9, 15.4, 52.7, 13.0 and 16.2 K for Nd^{3+}, Gd^{3+}, Dy^{3+}, Er^{3+} and Yb^{3+}, respectively. To the best of our knowledge, the Nd^{3+} and Yb^{3+} materials are the first examples of 3D- and 2D-MOFs, respectively, that show slow relaxation of magnetization.

Introduction

Metal-organic frameworks (MOFs) are a relatively new class of materials that have received great interest due to their structural and topological diversity, as well as to the properties that arise from their structural features.[1] In particular, the study of Lanthanide-based MOFs has evolved enormously in areas such as luminescence,[2] gas adsorption,[3] optical storage[4] and magnetism.[5] MOFs are obtained by the self-assembly of metal ions or clusters with appropriate bridging organic ligands. Still, there is a great interest in the design and preparation of new MOFs based on novel linkers conferring interesting properties. In the last years, we have designed and synthesized novel Lanthanide-MOFs with different tetrazolate derivate ligands with interesting luminescent properties.[6] We have also designed novel organic ligands to construct interesting single-molecule magnets based on dysprosium, showing interesting effective energy barriers.[7] Following these works, we report here the design and synthesis of a new family of 3D-MOFs and one 2D-based on the 9,10-anthracenedicarboxylic acid (*H_2ant*), where its anionic form (*ant*)$^{-2}$ acts as linker. Among various ligands, the versatile benzene-based carboxylic acid ligands, as for example 1,4-benzenedicarboxylic acid (H_2BDCA),[8] have been well used in the preparations of various carboxylate complexes owing to their rich variety of coordination modes. However, in this regard, the use of carboxylic acid ligands with bulky anthracene skeleton to construct functional carboxylate compounds has been less investigated so far. In this work, this multidentate bridging dianionic ligand (Scheme I) has been synthesized *in situ* by soft solvothermal routes by using oxidation of 9,10-anthracenedicarbonitrile ligand (Scheme II). *H_2ant* has been successfully used in previous works to prepare a series of transition metal complexes exhibiting magnetic and luminescent properties[9] but, to the best of our knowledge, there is only one MOF based on lanthanide ions, specifically lanthanum.[10] For this reason, we decided to prepare lanthanides-based MOFs using this ligand, and to study their luminescence and magnetic properties. Thanks to its extended aromaticity, (*ant*)$^{-2}$ is a good candidate for enhanced emissive properties, which are in principle tunable by coordination to metal with different chemical environments. Herein, we report the synthesis, structure, porosity, luminescence and magnetic properties of the 3D-MOFs $\{[Ln(ant)_{1.5}(DMF)_2]\cdot(DMF)\}_n$ (Ln = Pr (**1**), Nd (**2**), Gd(**3**), Tb (**4**), Dy (**5**), Er (**6**) and the 2D-MOF $\{[Yb(ant)(NO_3)(DMF)_2]\cdot(DMF)_{0.33}\}_n$ (**7**), demonstrating the potential of this dicarboxylate linker to construct new MOFs with interesting properties.

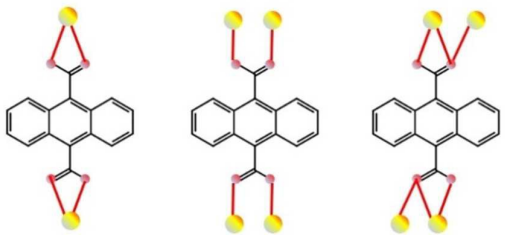

Scheme I. Different coordination modes exhibited by anthracenedicarboxylate linker in these materials.

[a] Dept. of Inorganic Chemistry, University of Granada, 18071, Granada, Spain. E-mail: ecolacio@ugr.es, antonio5@ugr.es
[b] Dept.of Applied Chemistry, Chemistry Faculty, The University of the Basque Country UPV/EHU, 20018, Donostia-San Sebastián, Spain. E-mail: josemanuel.seco@ehu.es
[c] Dept. of Chemical Engineering & Biotechnology, University of Cambridge, United Kingdom.

† Footnotes relating to the title and/or authors should appear here.
Electronic Supplementary Information (ESI) available: [Crystal Data, luminescence measurements, PSD Calculation and Magnetic Properties]. See DOI: 10.1039/x0xx00000x. *CCDC* numbers are 1421044-1421048 and 1054115.

Results and discussion

Description of the structures

The hydrothermal reaction (Scheme II) of the appropriate lanthanide nitrate (2 mmol) with 9,10-anthracene-dicarbonitrile (3 mmol) in dimethylformamide (10 ml) at 95 ºC for 24 h produced prismatic crystals of different MOFs.[11] The crystal structures were determined using single crystal X-ray crystallography.[12] Compounds **1**-**7** crystallize in the triclinic space group *P-1*. Compounds **1**-**6** are isostructural materials and the structure of **5** is described as example. The 3D-MOF structure of **5** is described by dysprosium dinuclear units (Figure 1) bridged by six different $(ant)^{-2}$ linkers. Within these dimers, Dy(III) ions are connected by four different $(ant)^{-2}$ ligands. In this material, $(ant)^{-2}$ ligand shows three different coordination modes: a) bis-chelating interdinuclear mode; b) bis-bridging intradinuclear mode; c) bis-η–O,O´–μ–O,O bridging/chelating intradinuclear mode (Scheme I). It should be noted that the presence of these three coordination modes of the $(ant)^{-2}$ ligand in the same material has not been reported previously for coordination compounds.

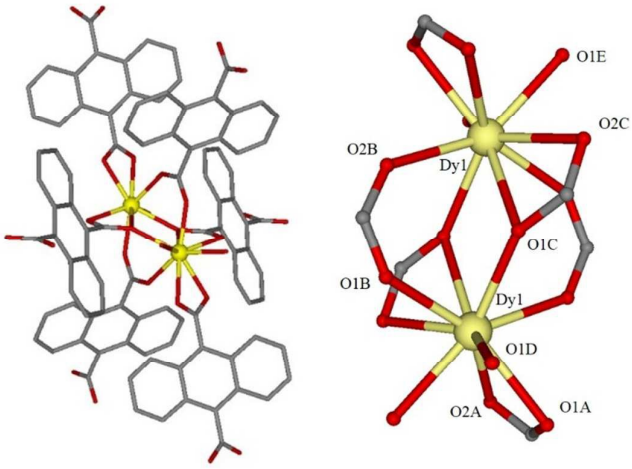

Figure 1. Left: Dinuclear entity formed by two dysprosium atoms and six anthracene dicarboxylate linkers. Right: Dysprosium coordination polyhedral. Hydrogen atoms have been omitted for clarity. O=red, C=grey, Dy=yellow.

The distortion of the DyO_9 coordination polyhedron is induced mainly by the different angles O1C-Dy-O2C, O1A-Dy-O2A (51.53(6) and 53.51(6)º, respectively) and Dy-O1C-Dy angle (107.57(6)º) generated by the carboxylate groups in the dimeric unit. The Dy^{III} atom exhibits a DyO_9 coordination environment which is made of seven oxygen atoms pertaining to five different $(ant)^{-2}$ ligands and two oxygen atoms (O1D and O1E) belonging to two DMF coordinated molecules. The 3D-MOF (Figure 2) presents channels along *b* axis with DMF solvent molecules inside. Gas adsorption analysis of N_2 at 77 K on the activated sample of **5** revealed no appreciable porosity.

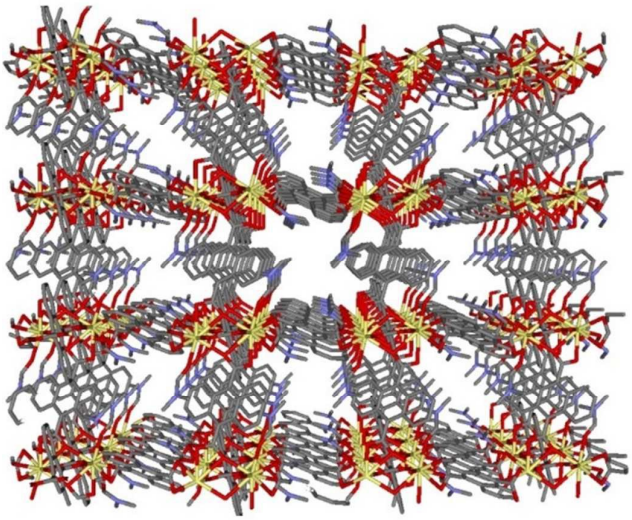

Figure 2. View down the *b* axis of the channels in compound **5**. DMF solvent molecules and hydrogen atoms have been omitted for clarity. Color code N = blue, O = red, C = grey, Dy = yellow.

The $Dy–O_{carb}$ bond distances are in the range 2.3046(17)-2.5439(18) Å whereas the $Dy–O_{DMF}$ distances are 2.3678(19) and 2.4005(19) Å. Within three-dimensional coordination polymer, the intradinuclear Dy···Dy distance is 3.9962(3) Å while interdinuclear Dy···Dy distances are in the range 10.745-11.803 Å.

Compound **7** crystallizes in the triclinic space group *P-1*. The 2D-MOF structure is composed of Yb(III) dimers connected by carboxylate groups of four different $(ant)^{-2}$ ligands that show a bis-chelating interdinuclear and a bis-bridging intradinuclear coordination modes. Thus, Yb-MOF can be described by ytterbium dinuclear units bridged by four different $(ant)^{-2}$ linkers but, in this case, the presence of nitrate anions and DMF coordination molecules stopping the propagation of the structure 2D to 3D (Figure 3).

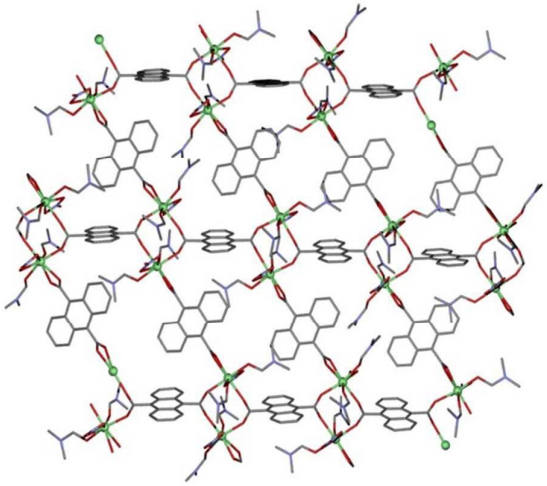

Figure 3. Normal view to [111] of the sheets in compound **7**. Hydrogen atoms have been omitted for clarity. Color code N = blue, O = red, C = grey, Yb = green.

Luminescence Properties

The conjugated π-systems of the anthracene rings are interesting in fluorescent materials.[13] For this reason, we have studied the luminescence properties of **1**–**7** as well as the free ligand at room temperature. The *H_2ant* ligand displays moderate luminescence in the solid state at λ_{em} = 518 nm upon excitation at λ_{exc} = 444 nm. Upon excitation at λ_{exc} = 380, compounds **1**-**7** exhibit intense luminescent emissions at λ_{em} *ca.* 430, 480 and 525 nm (Figure 4). Similar values have been reported for a lanthanum complex containing *H_2ant* ligand.[10] Moreover, upon excitation at 440 nm, **2** and **4** exhibit the typical emission bands of Nd^{3+} and Tb^{3+} ions, respectively (Figure S1). In the case of **2**, emission spectrum was measured in the 800–1100 nm range and the resulting two major peaks should be assigned to the $^4F_{3/2}/^4I_J$ (J=9/2 and 11/2) transitions, $^4F_{3/2}/^4I_{9/2}$ (870 nm), $^4F_{3/2}/^4I_{11/2}$ (1160 nm). For Tb^{3+} material, emission spectrum was measured in the 500–700 nm range and the resulting three major peaks should be assigned to the $^5D_4/^7F_J$ (J=3–6) transitions, $^5D_4/^7F_5$ (530 nm), $^5D_4/^7F_4$ (570 nm), $^5D_4/^7F_3$ (605 nm).

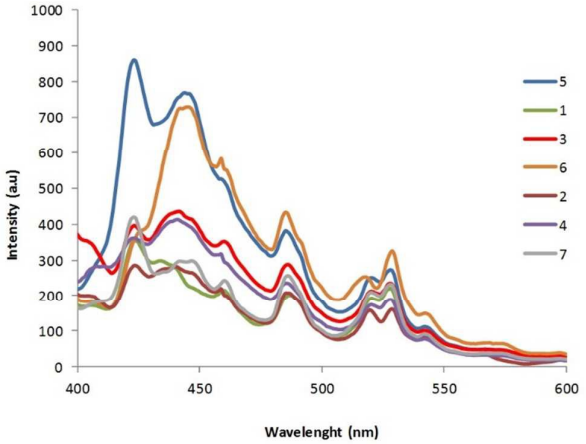

Figure 4. The emission spectra of compounds **1**-**7** after excitation at 380 nm in solid state at room temperature.

Magnetic Properties

The magnetic properties of compound **1**-**7** were measured in the temperature range 2–300 K under an applied magnetic field of 1000 Oe and are given as the temperature dependence of $\chi_M T$ product (χ_M is the molar susceptibility per Ln^{3+} atom) in Figure 5 top, whereas the field dependence of the magnetization at 2 K for complexes **1**-**7** is given in Figure 5 bottom. The room temperature $\chi_M T$ values are close to those expected for one isolated Ln^{3+} ion using the free ion approximation (Table 1).

We are going to start with the analysis of the magnetic properties of **3**. On cooling from room temperature, the $\chi_M T$ remains almost constant to 20 K (8.75 $cm^3mol^{-1}K$) and then sharply decreases to reach a value of 8.05 $cm^3mol^{-1}K$ at 2 K. The decrease of the $\chi_M T$ at low temperature is due to very weak antiferromagnetic $Gd^{III}\cdots Gd^{III}$ interactions and/or zero-field splitting effects of the Gd^{III} ions. In order to estimate the value of the magnetic exchange coupling in **3** we have used a very crude model, in which dinuclear Gd_2 units, with an intradinuclear magnetic coupling described by the *J* parameter, interact through *(ant)*$^{-2}$ ligands.

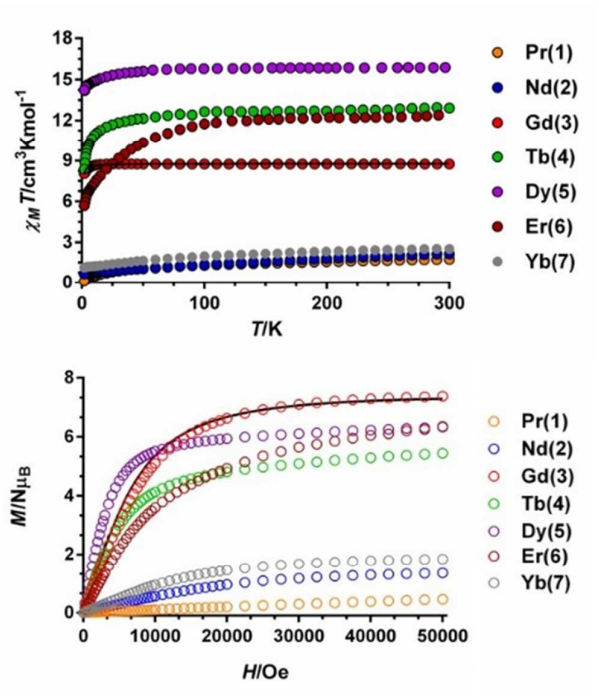

Figure 5. Top: Temperature dependence of the χ_MT product for compounds **1**-**7** in the presence of an external magnetic field H = 0.1 T. The black solid line shows the best fit of the experimental data for compound **3** with the Hamiltonian indicated in the text. Bottom: Temperature dependence of the magnetization at T = 2 K for compounds **1**-**7**. Solid lines corresponds to the Brillouin function for S = 7/2.

Table 1.- Direct current magnetic data for **1**-**7**

Compound	Spin-orbit Ground state of the Ln^{3+} ion	$\chi_M T$ theoretical[a]/ at 300 K / at 2K ($cm^3mol^{-1}K$)
1	$^3H_4$, g_J =4/5	1.60/1.74/0.11
2	$^4I_{9/2}$, g_J =8/11	1.64/2.14/0.67
3	$^8S_{7/2}$, g_J =2	7.88/8.75/8.05
4	$^7F_6$, g_J =3/2	11.82/12.91/8.38
5	$^6H_{15/2}$, g_J =4/3	14.17/15.88/1.99
6	$^4I_{15/2}$, g_J =6/5	11.48/12.42/5.7
7	$^2F_{7/2}$, g_J =8/7	2.57/2.51/1.14

[a] $\chi_M T = \frac{N\beta^2}{3k}\{g_J^2 J(J+1)\}$

The interdinuclear interactions, which can be calculated by using the molecular field theory, are described by the term zJ'. Taking into account these considerations, the magnetic susceptibility data were fitted with the following isotropic Hamiltonian:

$$\boldsymbol{H} = -JS_{Gd1}S_{Gd2} - zJ' < S_z > \boldsymbol{S_z}$$

The best fitting parameters were J = -0.02(1) cm^{-1}, $zJ' \sim 0$ and g = 2.111(1). These results show that the antiferromagnetic interactions between the Gd^{III} ions through the *(ant)*$^{-2}$ bridging ligands (and the ZFS effects if exist) are very weak. In fact, the isothermal magnetization curve does not deviate from the Brillouin function for S = 7/2 and g = 2.1. Similar values have been observed for other carboxylate-bridged Gd^{III} polynuclear complexes.[14] The $\chi_M T$ product for the other complexes decrease with decreasing temperature, first slowly down to 100 K and then quickly in the case of compounds **4**-**6** and progressively from room temperature in the case of complexes **1**, **2** and **7**. This behavior is due to a combination of the thermal depopulation of the *mj* sublevels of the $^{2S+1}\Gamma_J$ ground state of the Ln^{3+} ions, which is split by the effects of the crystal field, and probably very weak $Ln^{3+}\cdots Ln^{3+}$ antiferromagnetic interactions.

In order to know if these complexes show slow relaxation of the magnetization, we performed dynamic alternating-current (ac) magnetic measurements as a function of both temperature and frequency. Under zero-external field, only compound **5** showed a weak frequency dependence of the out-of-phase signal, χ''_M, but without a net maximum above 2 K at a frequency as high as 10000 Hz. This behavior may be due to fast resonant zero-field quantum tunneling of the magnetization (QTM), which leads to a flipping rate that is too fast to observe the maximum in the χ''_M above 2 K. When the *ac* measurements were performed in the presence of a small external *dc* field of 1000 Oe, compounds **2**, **3, 5**, **6** and **7** (Figures 6-9 and S2) exhibited slow relaxation of the magnetization.

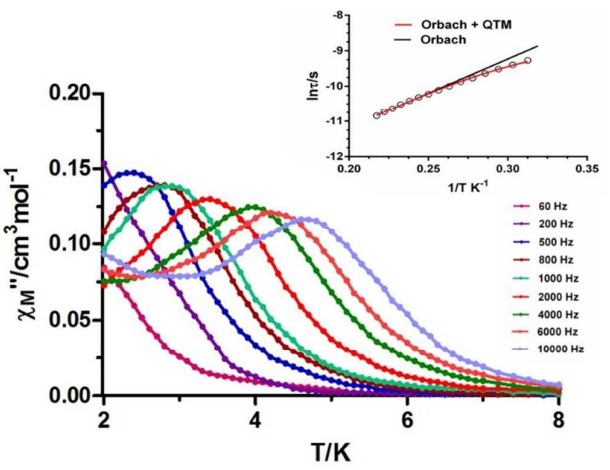

Figure 6. Temperature dependence of out-of-phase χ''_M components of the *ac* susceptibility for complex **2** under an external field of 1000 Oe. Inset: Arrhenius plots of relaxation times of **2** (black line). The red line represents the best fitting of the experimental data to the Orbach plus QTM.

It should be noted that compounds **2** and **3** show two relaxation processes below 3 K as can be seen in the Cole-Cole and χ''_M vs. frequency plots (Figures S3 and S4).

In the case of **2**, the fast relaxation process is probably due to QTM that is not fully suppressed by the application of the external field of 1000 Oe as can be seen by the tail at low temperature in the χ''_M vs. T plot (see Figure 6).

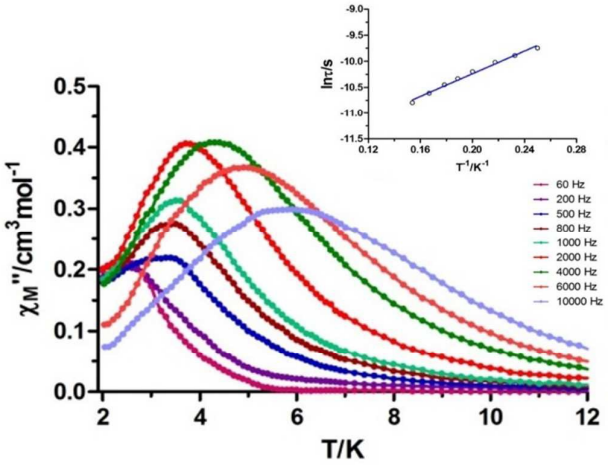

Figure 7. Temperature dependence of out-of-phase χ''_M component of the *ac* susceptibility for complex **3** under an external field of 1000 Oe. **Inset:** Arrhenius plots of relaxation times of **3**. The blue line represents the best fitting of the experimental data to the Arrhenius equation.

The relaxation times could only be extracted from the frequency-dependent susceptibility data for the slow relaxation process, as the faster one mainly appears above 10 KHz, the limit of our instrument. We have fitted the temperature dependence of the relaxation times for the slow process to an equation that considers the simultaneous presence of both the thermal and QTM processes (eq. 1), affording the parameters indicated in Table 2. These parameters are very close to those obtained for the unique Nd 1D-polymeric complex so far reported that present this type of behavior.[15]

$$\tau^{-1} = \tau_{QT}^{-1} + \tau_0^{-1} exp\left({}^{U_{eff}}/_{kT}\right) \quad Orbach + QTM\ (eq.1)$$

In the case of the Gd^{III} complex **3**, also two relaxation processes are observed (Figures 7, S3 and S4). Relaxation times (τ) for the slow relaxation process (SR) could not be accurately extracted, however, the τ values for the fast relaxation process (FR) could be fitted in the high temperature region to a Arrhenius plot, affording the effective energy barrier for the reversal of the magnetization and τ_0 values indicated in Table 2.

Table 2. Δ and τ_0 values for compounds **2**, **3**, **5, 6** and **7**.

Compound	Δ (K) at H = 1000 Oe	τ_0 (s)	τ_{QTM} (s)
2	22.9 (19.3)[a]	$1.57\cdot10^{-7}$($2.96\cdot10^{-7}$)	0.002
3	15.4	$7.65\cdot10^{-7}$	
5	52.7	$2.71\cdot10^{-7}$	
6	13.0	$1.5\cdot10^{-6}$	
7	16.2 (13.0)[a]	$4.3.10^{-8}$($1.1.10^{-8}$)	0.0001

[a] In brackets the values extracted from the Arrhenius law using high temperature data.

The FR process cannot be assigned to an Orbach mechanism as the U_{eff} is much larger than the expected anisotropic energy barrier (Gd^{III} is a rather isotropic ion and its magnetic anisotropy is negligible). The inverse of the FR time can be fitted to the equation $\tau^{-1} = AT^2$ (see Figure S5). Such temperature dependence can be explained, as in other Gd^{III} complexes, by a resonant phonon trapping (RTP) mechanism, through a phonon-bottleneck process. Similar U_{eff} values has been observed for other polymeric Gd(III) complexes.[15] The SR at low temperature is probably due to an Orbach and/or direct process, which arises from the lifting of the Kramers degeneracy of the Gd^{III} ground state by the static magnetic field, giving rise to a multi-level systems with slow relaxation.[15,16] This static bias field-induced SR process seems to be a quite general phenomenon for anisotropic as well as isotropic lanthanide containing systems.

The Arrhenius plot for **5** and **6** in the high temperature range (8-11 K) and (2-4 K) affords the U_{eff} and τ_o values for the Orbach process (see Table 2). It should be noted that for these complexes the temperature dependence of the relaxation times could not be fitted to the equation that takes into account the presence of both the Orbach and QTM processes. The Cole–Cole plots for these two complexes show α values 0.30 (7.5 K) - 0.13 (11 K) and 0.20 (2.4 K) - 0.04 (4.8 K) ranges, respectively, thus suggesting the existence of multiple relaxation processes (Figure S6). This fact is in agreement with the broad frequency-dependent peaks observed for these complexes (Figures 8, S2 and S7). Similar behaviors have been shown previously by 3D-Dy and 3D-Er MOFs.[17]

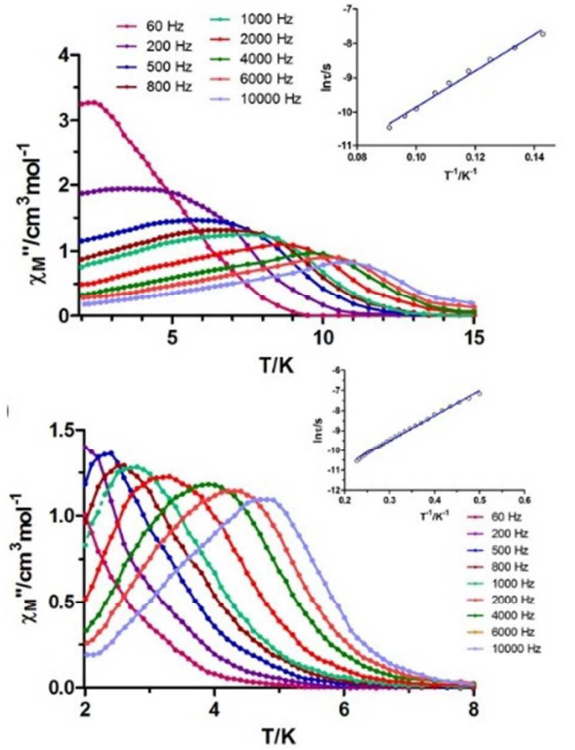

Figure 8. Temperature dependence of the out-of-phase χ''_M components of the *ac* susceptibility for complex **5** (top) and **6** (bottom) under an external field of 1000 Oe. Inset: Arrhenius plots of relaxation times of **5** (blue line, up) and **6** (blue line, bottom). The blue line represents the best fitting of the experimental data to the Arrhenius equation.

Finally, the Arrhenius plot in the 2.5 K-3 K for compound **7** afforded the U_{eff} and τ_0 values indicated in Table 2 (Figure 9). The fit of the relaxation times to an equation that considers the simultaneous presence of both the thermal and QTM processes give rise to an increase in U_{eff} and a decrease in τ_0 with regard to those extracted taking into account only the Orbach process, as expected. It should be noted that for most part of the Yb^{III} complexes, Raman relaxation processes have been proposed.[18] In view of this, relaxation times were fitted to an equation that considers the simultaneous presence of both the Raman and QTM processes (eq. 2), affording the parameters B = 273, n = 5.5, τ_{QTM} = 0.0001s.

$$\tau^{-1} = BT^n + \tau_{QT}^{-1} \quad Raman + QTM \ (eq.2)$$

In general n = 9 for Kramers ions, but depending on the structure of the levels, *n* values between 1 and 6 can be considered as acceptable. The obtained U_{eff} values are slightly higher but in good agreement with the obtained value for the unique Yb based 3D MOF exhibiting slow relaxation of the magnetization reported so far (5.78 K).[19]

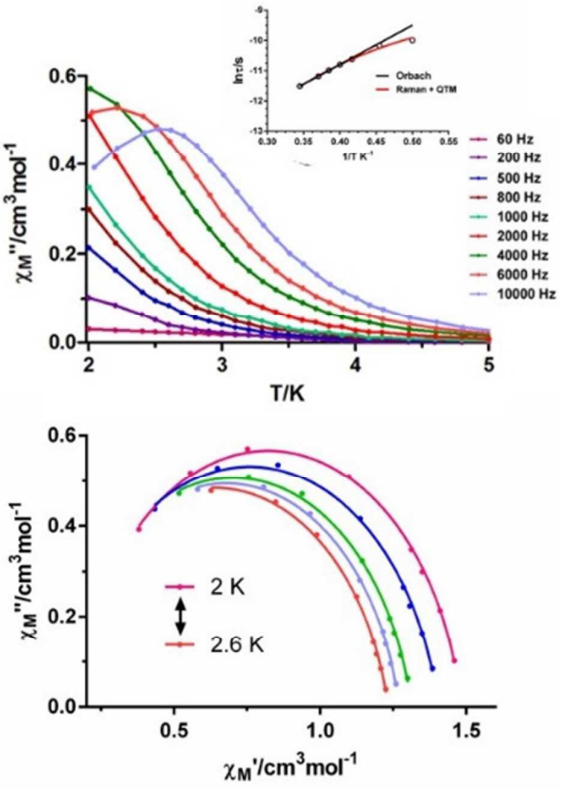

Figure 9. Top: Temperature dependence of the out-of-phase χ''_M component of the ac susceptibility for complex **7** under an external field of 1000 Oe. Inset: Arrhenius plots of relaxation times of **7** (black line). The red line represents the best fitting of the experimental data to the Raman plus QTM. The curve corresponding to the Orbach plus QTM is almost coincident with that for Raman plus QTM. Bottom: Cole-Cole plots under 1000 Oe external field for **7**. Solid lines represent the best fits to the generalized Debye model

Conclusion

In conclusion, a novel family of 3D-MOFs (2D in the case of the Yb compound) based on lanthanide ions and the linker 9,10-anthracenedicarboxylate have been synthesized and crystallographically characterized. The 9,10-anthracenedicarboxylate is a versatile ligand that exhibits different coordination modes in these compounds. Interestingly, the Nd^{3+}, Gd^{3+}, Dy^{3+}, Er^{3+} and Yb^{3+} complexes exhibit field-induced slow magnetic relaxation. The mechanism of their relaxation processes have been proposed from the data extracted from *ac* susceptibility measurements. To the best of our knowledge, the Nd^{3+} and Yb^{3+} materials are the first examples of 3D- and 2D-MOFs, respectively, that show slow relaxation of magnetization.

Experimental Section

Materials and physical measurements

All reagents were obtained from commercial sources and used as received. Elemental (C, H, and N) analyses were performed on a Leco CHNS-932 microanalyzer. IR spectra of powdered samples were recorded in the 400–4000 cm^{-1} region on a Nicolet 6700 FTIR spectrophotometer using KBr pellets.

Magnetic measurements

Variable-temperature magnetic susceptibility (2-300 K) under an applied field of 1000 Oe and magnetization measurements at 2 K and different magnetic fields (0-50 kOe) were carried out with a Quantum Design SQUID MPMS XL-5 device.

Alternating current magnetic measurements were performed on a PPMS (Physical Property Measurement System) - Quantum Design Model 6000 magnetometer by using an oscillating ac field of 3.5 Oe and ac frequencies ranging from 60 to 10000 Hz. The experimental susceptibilities were corrected for the sample holder and diamagnetism of the constituent atoms by using Pascal's tables.

Luminescence measurements

A Varian Cary-Eclipse Fluorescence Spectrofluorimeter was used to obtain the fluorescence spectra. The spectrofluorimeter was equipped with a xenon discharge lamp (peak power equivalent to 75 kW), Czerny-Turner monochromators, R-928 photomultiplier tube which is red sensitive (even 900 nm) with manual or automatic voltage controlled using the Cary Eclipse software for Windows 95/98/NT system. The photomultiplier detector voltage was 700 V and the instrument excitation and emission slits were set at 5 and 5 nm, respectively.

Adsorption Analysis

N_2 adsorption isotherms were undertaken at 77 K using a Micromeritics ASAP 2020 instrument. Samples were activated at 393 K for 8 hours previous to the adsorption measurement.

Crystallographic refinement and structure solution

Prismatic crystals for **1-5** and **7** were mounted on a glass fibre and used for data collection on a Bruker D8 Venture with Photon detector equipped with graphite monochromated *MoKα* radiation (λ=0.71073 Å). The data reduction was performed with the APEX2[20] software and corrected for absorption using SADABS.[21]

Table 1. Crystallographic Data and Structural Refinement Details for **1-5** and **7**

compound	1	2	3	4	5	7
chemical formula	$C_{33}H_{33}N_3O_9Pr$	$C_{33}H_{33}N_3O_9Nd$	$C_{33}H_{33}N_3O_9Gd$	$C_{33}H_{33}N_3O_9Tb$	$C_{33}H_{33}N_3O_9Dy$	$C_{69}H_{73}N_{10}O_{28}Yb_3$
CCDC	1421047	1421048	1421044	1421045	1054115	1421046
M/gmol^{-1}	756.53	759.86	772.87	774.54	778.12	2009.49
T (K)	100	100	100	100	100	100
λ/Å	0.71073	0.71073	0.71073	0.71073	0.71073	0.71073
cryst syst	triclinic	triclinic	triclinic	triclinic	triclinic	triclinic
space group	*P-1*	*P-1*	*P-1*	*P-1*	*P-1*	*P-1*
a/ Å	10.4477(6)	10.471(5)	10.3541(12)	10.468(5)	10.3803(5)	13.5512(16)
b/ Å	11.4945(7)	11.359(5)	11.3680(13)	11.356(5)	11.3508(6)	13.6376(16)
c/ Å	12.9583(7)	13.093(6)	12.9160(15)	13.089(6)	12.9894(7)	21.667(2)
α/deg	106.639(2)	107.541(5)	72.8590(10)	107.539(5)	72.4350(10)	106.851(4)
β/deg	90.322(2)	90.084(6)	90.0280(10)	90.086(6)	89.8670(10)	97.131(4)
γ/deg	93.194(2)	92.355(6)	87.2320(10)	92.356(6)	87.3720(10)	91.457(4)
V/ Å^3	1488.32(15)	1483.5(11)	1450.9(3)	1482.1(12)	1457.47(13)	3794.7(8)
Z	2	2	2	2	2	2
ρ(g cm-3)	1.688	1.701	1.769	1.736	1.773	1.759
μ(mm-1)	1.700	1.813	2.350	2.449	2.628	3.755
Unique reflections	21270	11612	16568	16407	17403	173864
R(*int*)	0.083	0.075	0.057	0.088	0.020	0.046
GOF on F^2	1.045	0.978	0.943	0.911	1.073	1.069
R1 [$I > 2\sigma(I)$]	0.050	0.048	0.045	0.058	0.024	0.062
wR2 [$I > 2\sigma(I)$]	0.094	0.102	0.097	0.112	0.058	0.125

[a] $R(F) = \sum||F_o| - |F_c||/\sum|F_o|$, $wR(F^2) = [\sum w(F_o^2 - F_c^2)^2/\sum wF^4]^{1/2}$

Crystal structures were solved by direct methods using the SIR97 program[22] and refined by full-matrix least-squares on F^2 including all reflections using anisotropic displacement parameters by means of the WINGX crystallographic package.[23] Generally, anisotropic temperature factors were assigned to all atoms except for hydrogen atoms, which are riding their parent atoms with an isotropic temperature factor arbitrarily chosen as 1.2 times that of the respective parent. It should be noted that all crystals undergo degradation when they are removed from the mother liquor which has a high impact on the quality of the data. Several crystals of compound **7** were measured and the structure was solved from the best data we were able to collect. Attempts to solve disorder problems with one DMF crystallization molecule failed in compounds **1**-**7**. Instead, a new set of F^2 (hkl) values with the contribution from solvent molecule withdrawn was obtained by the SQUEEZE procedure implemented in PLATON-94.[24] Final R(F), wR(F2) and goodness of fit agreement factors, details on the data collection and analysis can be found in Table 1. CCDC numbers are 1421044-1421048 and 1054115. These data can be obtained free of charge from The Cambridge Crystallographic Data Centre via www.ccdc.cam.ac.uk/data_request/cif

Compound **6** is isostructural to **5**. We realized a LeBail refinement (Figure S8) with TOPAS software to establish the purity and the unit cell of the powders pertaining to this material.

Syntheses of compounds

Initially, we carry out the synthesis by oxidizing 9,10-anthracenedicarbonitrile to 9,10-anthracenedicarboxylic acid (Scheme II). Then, we saw that using directly 9,10-anthracenedicarboxylic acid, the reaction yields were increased and improved purity.

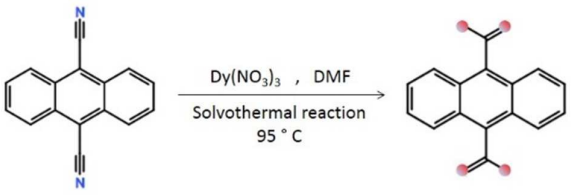

Scheme II. Soft solvothermal route by using oxidation of 9,10-anthracenedicarbonitrile ligand.

Synthesis of $\{[Ln(Ant)_{1.5}(DMF)_2].(DMF)\}_n$ (Ln = Pr(**1**), Nd(**2**), Gd(**3**), Tb(**4**), Dy(**5**), Er(**6**)) and **$\{[Yb(ant)(NO_3)(DMF)_2]\cdot(DMF)_{0.33}\}_n$**.

Compounds **1**-**7** were obtained by solvothermal methods through the following procedure: 0.008 g of H_2ant (0.033 mmol) were added to 2 mL of DMF. The resulting solution was sonicated for 10 minutes, and then a DMF solution (2 ml) containing the lanthanide nitrate hydrate [0.1 mmol, 0.044 (**1**), 0.044 (**2**), 0.045 (**3**), 0.045 (**4**), 0.044 (**5**), 0.044 (**6**) and 0.045 g (**7**)] were added. The reaction mixture was heated in a closed vial at 95°C in an oven for 24h. Pale yellow crystals were obtained. Yields: 19 (**1**), 25 (**2**), 21 (**3**), 18 (**4**), 23 (**5**), 19 (**6**) and 31% (**7**) based on Ln ion. Elemental Analysis of $C_{33}H_{33}N_3O_9Pr$ (**1**), calcd: C 52.39, H 4.40, N 5.55; found: C 52.70, H 4.68, N 5.17. Elemental Analysis of $C_{33}H_{33}N_3O_9Nd$ (**2**), calcd: C 52.16, H 4.38, N 5.53; found: C 52.54, H 4.63, N 5.21. Elemental Analysis of $C_{33}H_{33}N_3O_9Gd$ (**3**), calcd: C 51.28, H 4.30, N 5.44; found: C 51.45, H 4.39, N 5.61. Analysis of $C_{33}H_{33}N_3O_9Tb$ (**4**), calcd: C 51.17, H 4.29, N 5.43; found: C 51.52, H 4.60, N 5.11. Elemental Analysis of $C_{33}H_{33}N_3O_9Dy$ (**5**), calcd: C 50.94, H 4.27, N 5.40; found: C 51.23, H 4.58, N 5.11. Elemental Analysis of $C_{33}H_{33}N_3O_9Er$ (**6**), calcd: C 50.63, H 4.25, N 5.37; found: C 51.04, H 4.61, N 5.04. Elemental Analysis of $C_{66}H_{66}N_9O_{27}Yb_3$ (**7**), calcd: C 40.94, H 3.44, N 6.51; found: C 41.15, H 3.57, N 6.47.

Acknowledgements

This work was supported by the Junta de Andalucía (FQM-1484, and FQM-195, Project of excellence P11-FQM-7756), UPV/EHU Project GIU 14/01 and MEC of Spain (Project CTQ2011-24478 and CTQ2014-56312-P). I.O. is grateful to the Departamento de Educación, Universidades e Investigación del Gobierno Vasco for a predoctoral fellowship. The authors thank for technical and human support provided by SGIKER of UPV/EHU.

Notes and references

1.- O.K. Farha, A.O. Yazaydın, I. Eryazici, C.D. Malliakas, B.D. Hauser, M.G. Kanatzidis, S.T. Nguyen, R.Q. Snurr and J.T. Hupp, *Nat. Chem*., 2010, **2**, 944.
2.- H.-Y. Li, Y.-L. Wei, X.-Y. Dong, S.-Q. Zang and T.C.W. Mak, *Chem. Mater*, 2015, **27**, 1327.
3.- S. Biswas, H.S. Jena, S. Goswami, S. Sanda and S. Konar, *Cryst. Growth Des.,* 2014, **14**, 1287.
4.- P.-F. Shi, B. Zhao, G. Xiong, Y.-L. Hou and P. Cheng, *Chem. Commun*., 2012, **48**, 8231.
5.- J.J. Baldov, E. Coronado, A. Gaita-Ariño, C. Gamer, M. Giménez-Marqués and G. Mínguez-Espallargas, *Chem. Eur. J*., 2014, **20**, 10695.
6.- A. Rodríguez-Diéguez, A. Salinas-Castillo, A. Sironi, J.M. Seco and E. Colacio, *CrystEngComm*, 2010, **12**, 1876.
7.- J. Ruiz, A.J. Mota, A. Rodríguez-Diéguez, S. Titos, J.M. Herrera, E. Ruiz, E. Cremades, J. Pierre Costes and E. Colacio, *Chem. Commun*., 2012, **48**, 7916.
8.- (a) W.-M. Bu, L. Ye and Y.-G. Fan, *Inorg. Chem. Commun*., 2000, **3**, 194; (b) H. L. Zhu, X.-Y. Liu, X.-J. Wang, F. Yang, A. Usman and H. K. Fun, *Z. Anorg. Allg. Chem*., 2003, **629**, 1986.
9.- (a) C.S. Liu, J.J. Wang, Z. Chang, S.R. Batten, L.F. Yan and X.H. Bu, *Trends Inorg. Chem*., 2010, **10**, 81; (b) J.J. Wang, T.L. Hu and X.H. Bu, *CrystEngComm*, 2011, **13**, 5152.
10.- J.-J. Wang, Z. Chang and T.-L. Hu, *Inorg. Chim. Acta,* 2012*,* **385**, 58.
11.- *H_2ant* (0.33 mmol) was added to 2ml DMF. The resulting solution was sonicated for 10 minutes, and appropriate $Ln(NO_3)_3$ (0.1 mmol) in 2 ml DMF were added. The reaction mixtures were heated in a closed vial at 95°C in oven for 48h. Prismatic crystals of **1**-**7** were obtained (ESI).
12.- Compounds **1**-**6** are isostructural, consequently, they have very similar unit cell parameters. More information see ESI. Crystal data for **3**: $C_{33}H_{33}DyN_3O_9$, M = 778.12 g mol^{-1}; triclinic, *P-1*, a = 10.3803(5), b = 11.3508(6), c = 12.9894(7), α = 72.4350(10), β = 89.8670(10), γ = 87.3720(10). Crystal data for **7**: $C_{33}H_{33}DyN_3O_9$, M = 778.12 g mol^{-1}; triclinic, *P-1*, a = 10.3803(5), b = 11.3508(6), c = 12.9894(7), α = 72.4350(10), β = 89.8670(10), γ = 87.3720(10), V = 1457.47(13) Å^3.
13.- Q.-Y. Liu, Y.-L. Li, Y.-L. Wang, C.-M. Liu, L.-W. Dinga and Y. Liua, *CrystEngComm*, 2014, **16**, 486.
14.- L. Cañadillas-Delgado, O. Falbelo, J. Cano, J. Pasán, F. S. Delgado, F. Lloret, M. Julve and C. Ruiz-Pérez, *Cryst.Eng.Commun*. 2009, **11**, 2131.
15.- A. Arauzo, A. Lazarescu, S. Shova, E. Bartolomé, R. Cases, J. Luzón, J. Bartolomé and C. Turta, *Dalton Trans*. 2014, **43**, 12342.
16.- B. Liu, B.-W. Wang, Z.-M. Wang and S. Gao, *Science China*, 2012, **55**, 926.

17.- (a) Y. Wu, S. Zhan, L. Xu, W. Shi, T. Xi, X. Zhan and P. Zhou, *Chem. Commun*., 2011, **47**, 6027; (b) B. Liu, B.-W. Wang, Z.-M. Wang and S. Gao, *Science China*, 2012, **55**, 926.
18.- J. Ruiz, G. Lorusso, M. Evangelisti, E.K. Brechin, S.J. Pope and E. Colacio, *Inorg. Chem*., 2014, **53**, 3586.
19.- F. Zhang, P. Yan, X. Zou, J. Zhang, G. Hou and G. Li, *Cryst. Growth Des*., 2014, **14**, 2014.
20.- Bruker Apex2, Bruker AXS Inc., Madison, Wisconsin, USA, 2004.
21.- G.M. Sheldrick, SADABS, Program for Empirical Adsorption Correction, Institute for Inorganic Chemistry, University of Gottingen, Germany, 1996.
22.- A. Altomare, M. C. Burla, M. Camilla, G. L. Cascarano, C. Giacovazzo, A. Guagliardi, A. G. G. Moliterni, G. Polidori and R. Spagna, J. Appl. Crystallogr., 1999, 32, 115.
23.- (a) G. M. Sheldrick, SHELX-2014, Program for Crystal Structure Refinement, University of Göttingen, Göttingen, Germany, 2014. (b) L. J. Farrugia, J. Appl. Cryst., 1999, 32, 837.
24.- Spek, A. L. PLATON-94 (V-101094), A Multipurpose Crystallographic Tool, University of Utrecht, The Netherlands, 1994.